ISSN (Print) 1226-1750
ISSN (Online) 2233-6656
Journal of Magnetics 22(3), 364-368 (2017) https://doi.org/10.4283/JMAG.2017.22.3.364

Micromagnetic Calculation of the Dynamic Susceptibility Spectra in LSMO ($La_{0.7}Sr_{0.3}MnO_3$) Ferromagnetic Nanopillars

D. Djuhana[1]*, L. Rohman[2], and D. H. Kim[3]

[1]*Departemen Fisika FMIPA Universitas Indonesia, Kampus UI Depok, Depok 16424, Indonesia*
[2]*Departemen Fisika FMIPA Universitas Jember, Jl. Kalimantan 37, Jember 68121, Indonesia*
[3]*Department of Physics, Chungbuk National University, Cheongju 28644, South Korea*

(Received 13 April 2017, Received in final form 2 July 2017, Accepted 17 July 2017)

In this study, we have systematically calculated the dynamic susceptibility spectra of LSMO ($La_{0.7}Sr_{0.3}MnO_3$) ferromagnetic nanopillars by means of a micromagnetic simulation. Simulation has been carried out for LSMO nanopillars consisted of disk and square shapes with respect to the height variation. The diameter of disk pillar and the length of square pillar were fixed to be 50 nm and the height of pillar were varied from 100 to 500 nm with increment of 50 nm. The exponential type magnetic pulses have been applied in the long axis and perpendicular to the initial spin configuration of the pillars. The dynamic susceptibility spectra of the pillar were determined by fast Fourier transform (FFT) based on the magnetization response. We have obtained the resonance frequency of the pillars from the imaginary part of the dynamic susceptibility spectra. Interestingly, the resonance frequency peak of the nanopillars increased as the height increased and followed the Kittel's resonance formula. It was found that the demagnetization energy from dipolar interaction mainly contributed to the frequency resonance of the nanopillars.

Keywords : micromagnetics, dynamic susceptibility, $La_{0.7}Sr_{0.3}MnO_3$ nanopillar

1. Introduction

For the last two decades, the perovskite-type manganese oxide $La_{1-x}A_xMnO_3$ (A=Sr, Ba, Ca) has been attracting much interest due to its potential application for magnetic random access memory (MRAM) and spintronic devices. For instance, it has been known that LSMO has a half-metal property exhibiting the colossal magnetoresistance (CMR), where the main properties of LSMO are mainly affected by parameters such as doping, magnetic and electric field, and strain [1]. Thus, understanding the LSMO properties and underlying mechanism becomes important both in fundamental and practical application. Recently, several reports have been addressed to the nanostructured LSMO properties, where interesting phenomena are found such as the controlling the spin configuration [2], inverted and giant exchange bias [3], and uniaxial anisotropy [4] of the nanostructured LSMO. However, very little has been known for LSMO with shape of nanopillars, where shape influence, different domain structures from films and bulks, and different spin wave resonance frequency are expected.

In this study, we calculate the susceptibility spectra of LSMO ferromagnetic nanopillars using a micromagnetic simulation. The LSMO nanopillars consisted of disk and square pillar shapes are systematically analyzed. By using Fourier transform, we calculate the susceptibility spectra based on the magnetization and the applied field. We focus on the imaginary part of the susceptibility spectra that related to the resonance frequency and also confirms that the Kittel's equation is valid for the resonance frequency. Corresponding behavior of the magnetic energy and the domain structure of the LSMO nanopillars are discussed.

2. Micromagnetic Procedure

We have systematically calculated the dynamic susceptibility spectra of the LSMO ferromagnetic nanopillars by a micromagnetic 3D OOMMF [5] based on the Landau-Lifshitz-Gilbert equation [6]. Two shape of LSMO nanopillars were considered in this simulation: the disk pillar

*Corresponding author: Tel: +62-21-786-3441
Fax: +62-21-787-2610, e-mail: dede.djuhana@sci.ui.ac.id

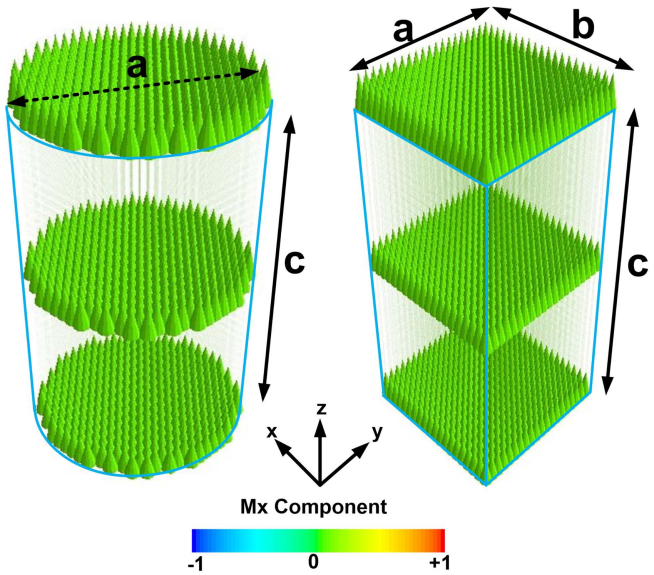

Fig. 1. (Color online) The geometry and shape of LSMO nanopillars corresponds to $a = b = 50$ nm and $c = 1000$ nm. The small external field is applied along the x direction perpendicular to z direction. The colour bar represents the magnetization in x component (Mx component).

and the square pillar. The diameter of the disk pillar was $a = 50$ nm, the length of square $a = b = 50$ nm, and the height of the pillars were $c = 1000$ nm, as illustrated in Fig. 1. For this purpose, we simulated the pillars with respect to the aspect ratio (a/c) from 2 to 20. The material parameters of LSMO were used [7]. The saturation magnetization was $M_s = 590 \times 10^3$ Am^{-1}, the exchange stiffness was $A = 5 \times 10^{-12}$ Jm^{-1}, and the anisotropy constant was $K = -0.3 \times 10^3$ Jm^{-3}. The simulation cell size was $2.5 \times 2.5 \times 2.5$ nm^3 and the damping constant was set to be $\alpha = 0.01$. Then, the small external field $H(t)$ $= 1000\ e^{-10^9 t}$ ($t \geq 0$, $H(t)$ in Am^{-1} and t in second) was applied along x-direction perpendicular to easy axis (z direction) of the pillars [8].

3. Results and Discussions

The dynamic susceptibility of LSMO pillars was determined based on the relation $\chi(\omega) = M(\omega)/H(\omega) = \chi(\omega)' - j\chi(\omega)''$ where $M(\omega)$ and $H(\omega)$ were the magnetization and the external field response in the frequency domain, respectively. The real $\chi(\omega)'$ and imaginary $\chi(\omega)''$ part of the susceptibility spectra of LSMO pillars were obtained by Fourier transform technique. In this study, we focused on the imaginary part of the susceptibility spectra because it related to the resonance frequency [9]. The imaginary part of LSMO pillar for the aspect ratio for 2, 5, 10, 15, and 20 are shown in Fig. 2(a). The frequency is observed in range of GHz both disk pillar and square pillar. To compare, we have also calculated the resonance frequency of LSMO pillars based on the Kittel's equation [10] as follow

$$\omega = \frac{\gamma}{2\pi}\sqrt{[H_0 + H_k + (N_y - N_x)M_s][H_0 + H_k + (N_z - N_x)M_s]} \quad (1)$$

where H_0 was the static field, $H_k = 2K/(\mu_0 M_s)$ was the anisotropy field, M_s was the saturation magnetization, and γ was the gyromagnetic ratio 2.21×10^5 mA^{-1}S^{-1}. The demagnetizing factors N_x, N_y, and N_z for square pillar was determined by Aharoni's equation [11] and the disk pillar based on Dao calculation [8]. Fig. 2(b) showed the peak frequency of the LSMO disk and square pillars from micromagnetic and Kittel's equation with respect to the aspect ratio. Interestingly, the micromagnetic calculation

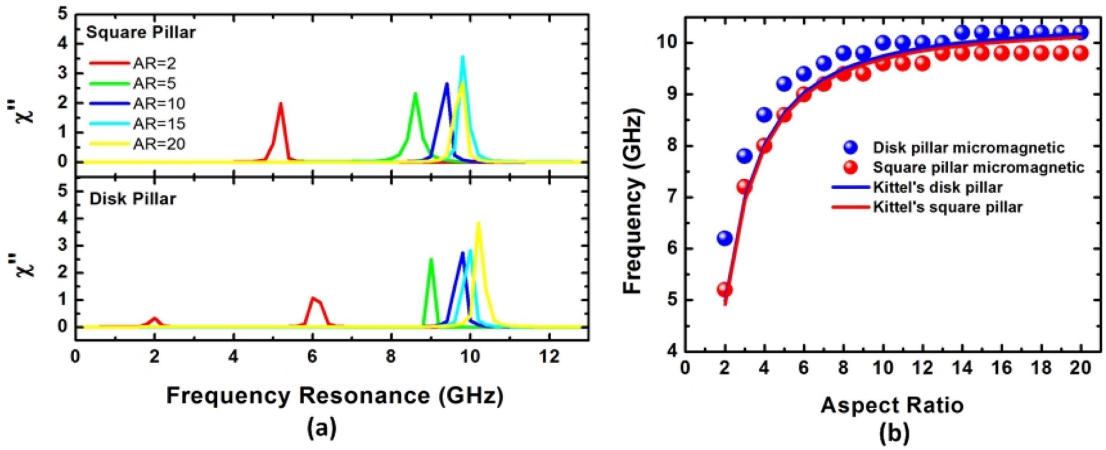

Fig. 2. (Color online) (a) The imaginary part of LSMO pillars for the aspect ratio 2, 5, 10, 15, and 20. (b) The frequency behaviour simulated (circular symbol) and fitting from the Kittel's equation (solid line) with respect to the aspect ratio.

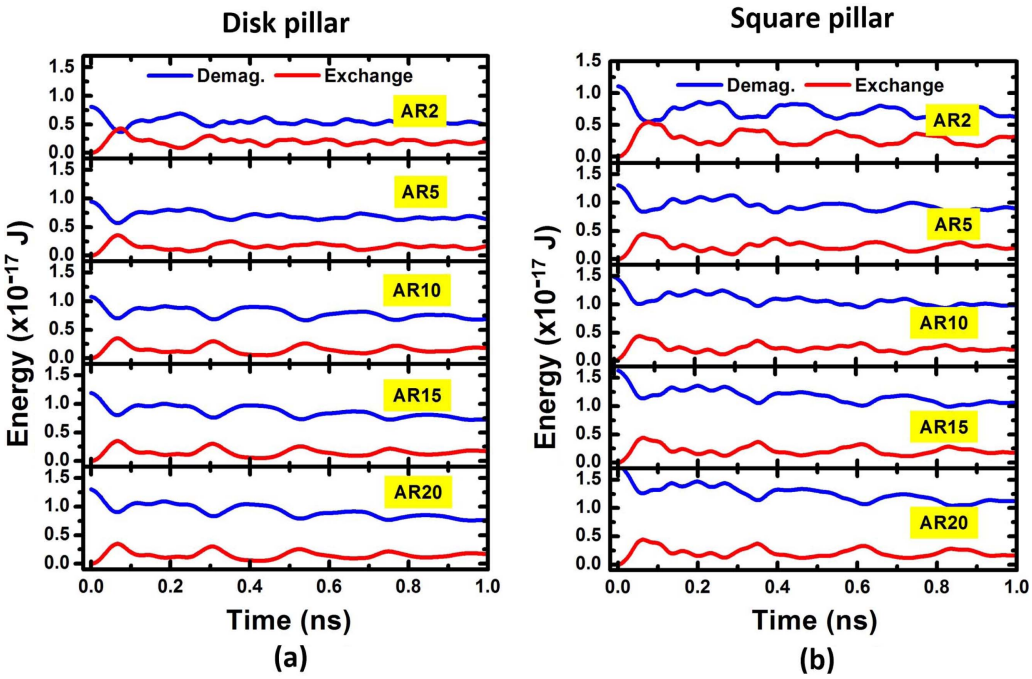

Fig. 3. (Color online) The demagnetization and the exchange energy profile corresponding to the aspect ratio 2, 5, 10, 15, and 20 for (a) the disk pillar and (b) the square pillar of LSMO samples.

showed the validity of the Kittel's prediction, with a trend of the frequency increasing as the aspect ratio of the pillars increased. We have also found the same trend in the case of disk pillar [8].

For further understanding, we have also investigated the magnetization energies both disk and square pillars. Fig. 3 shows the demagnetization and the exchange energies for the aspect ratio 2, 5, 10, 15, and 20. The demagnetization energy seems to dominate over the exchange energy. With increasing the aspect ratio, the demagnetization energy also increased and the exchange energy was observed to be relatively constant. As in the figure, it was found that the demagnetization energy of the square pillar was higher than that of the disk pillar. The demagnetization energy commonly depends on the volume of the material, where the volume of the square pillar was larger than the disk pillar. Thus, it is understandable that the demagnetization energy of the square pillar was higher than the disk pillar with increasing the aspect ratio. Then, we have also observed the demagnetization and the exchange energies for the aspect ratio 2, around time from 0.070 ns to 0.09 ns, as in Fig. 4.

Figure 4(a) shows the time-dependent demagnetization and the exchange energies for the disk pillar. Interestingly, the demagnetization energy decreased until $t = 0.075$ ns then increased again whereas the exchange energy increased then decreased around $t = 0.085$ ns. On the other hand, different behavior is observed in the case of the square pillar, where the exchange energy becomes close to the demagnetization energy and it did not show overlapping as in the case of the disk pillar (Fig. 4(b)). We have depicted the detailed domain structure of the pillars around time from 0.070 ns to 0.090 ns. Interestingly, it is observed that the vortex structure was formed for both the disk and square pillars. In the case of the disk pillar, the spin configuration in the vortex structure initially moved from the edge then to the center of the pillar, whereas the spin configuration in the vortex structure moved around the center of the pillar in the case of the square pillar.

The different spin configurational dynamics between the disk pillar and the square pillar is denoted directly by the resonance frequency behavior. As seen in detail in Fig. 2(a), the disk pillar sample exhibited two resonance frequencies at 2 GHz and 6 GHz for the case of the aspect ratio 2. On the other hand, the square pillar sample with the same aspect ratio only showed one resonance frequency at 5.2 GHz. The resonance frequency behavior of the LSMO pillar samples can be confirmed by the spin configuration and the magnetization energy profiles. We have presented the spin configuration image of the LSMO pillars in Fig. 5 for $t < 1$ ns with an increment of 0.25 ns. As the external field was switched on, the multidomain structures are formed for both the disk and the square

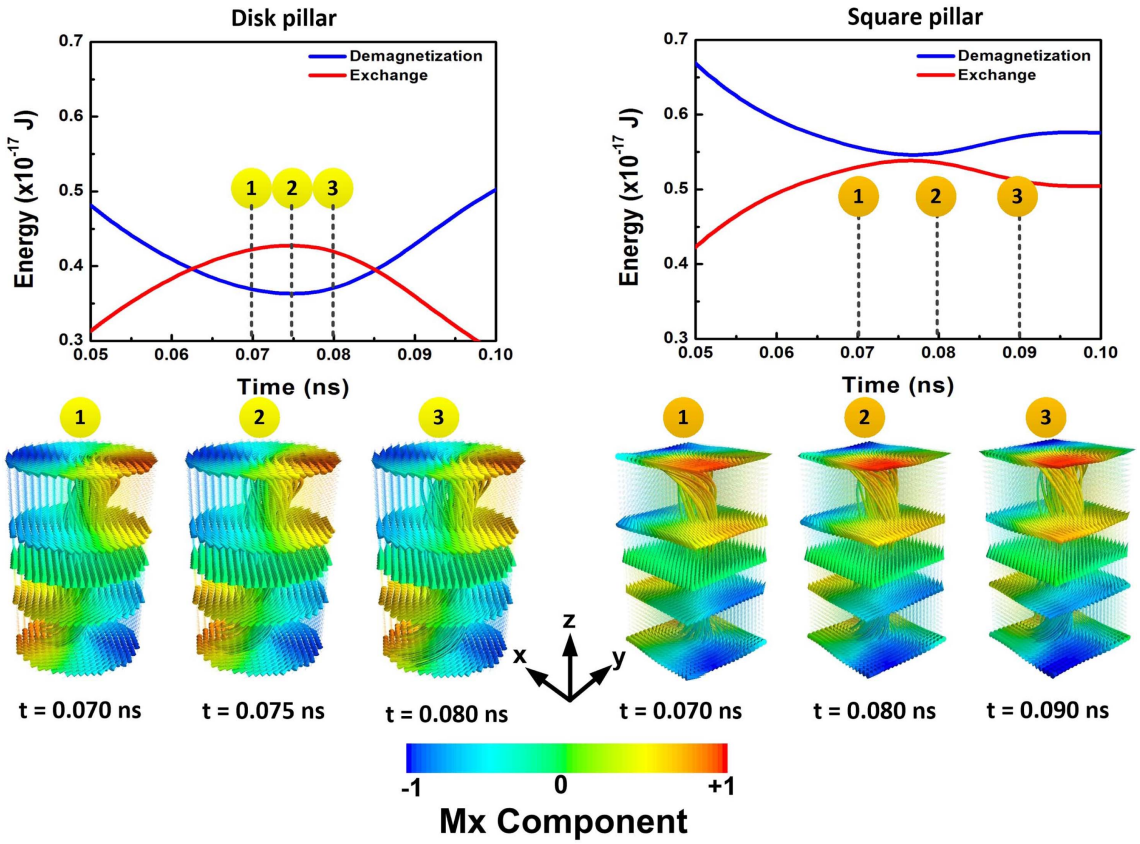

Fig. 4. (Color online) The demagnetization and exchange energy profile of the pillars for the aspect ratio 2. Bottom figures present the corresponding spin configurations at time t = 0.070, 0.075, and 0.080 ns for the disk pillar (left) and t = 0.070, 0.080, and 0.090 ns for the square pillar (right). The vortex structure moves from the edge to the center of the pillar (disk pillar) whereas the vortex structure moves around the center of the pillar (square pillar). The colour bar represents the magnetization in x component (Mx component).

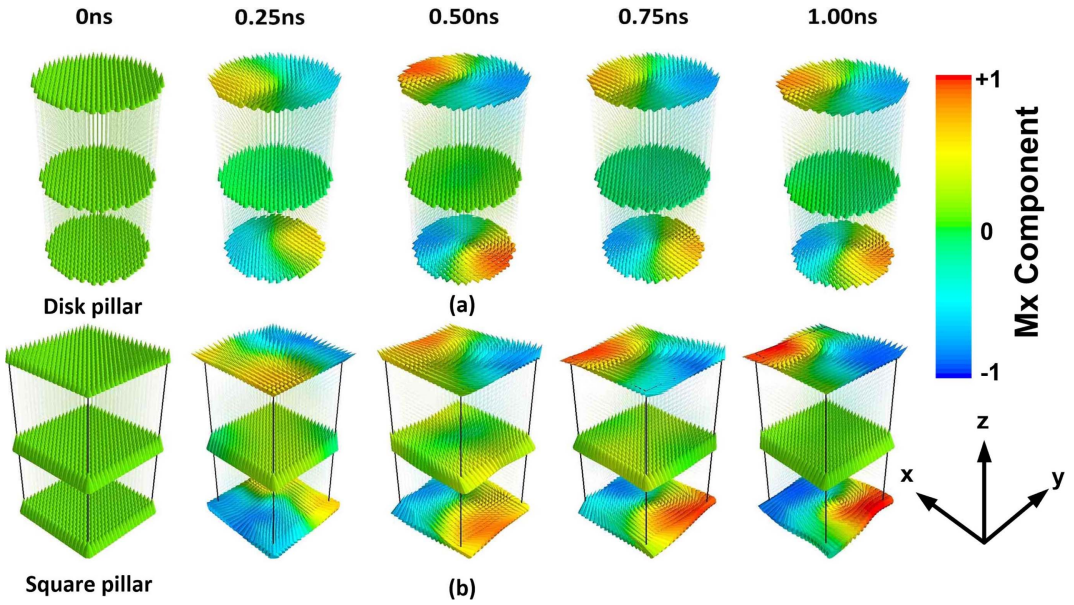

Fig. 5. (Color online) The domain structure of the pillars for the aspect ratio 2 until time 1 ns (a) the disk pillar and (b) the square pillar. The colour bar represents the magnetization in x component (Mx component).

pillars. The vortex structure also was formed from below of the pillars, then moving toward the middle and the top of the pillars. The spin configuration at middle of the pillars tends to align along the long axis of the pillars. In this middle pillar region, the demagnetizing field and the exchange interaction preserve the spin configuration to align along the long axis, thereby contributing to the observed resonance frequency behavior. Thus, our simulation results imply that the resonance frequency of the pillar is mainly originated from the dipolar interaction. Analysis of the magnetization energy such as the demagnetization and exchange energy together with corresponding domain structures allows us to understand the resonance frequency behavior simulated for the LSMO pillars. It has been found that the spin configuration of the LSMO pillars is consisted of two modes; first at the end of the pillar and the other at the middle of the pillar like single-domain structure, where the resonance frequency of the LSMO pillars was generated mainly from the middle part of the pillars.

4. Conclusion

In conclusion, our systematic micromagnetic investigation predicts the spin wave resonance spectra behavior of the LSMO pillars, where the resonance behavior overall follows the Kittel's equation. It is observed that the demagnetization energy mostly dominates over the exchange frequency with increasing the aspect ratio of pillars. The dynamic spin configuration is found to have two modes such as the vortex structure at the end of the pillar and the single-domain structure at the middle of the pillars. It is concluded that the dipolar interaction mostly contributes to determining the resonance frequency behavior of LSMO pillars.

Acknowledgement

This work was supported by Hibah Penelitian Unggulan Perguruan Tinggi (PUPT) Tahun 2017 (No. 2700/UN2.R3.1/HKP05.00/2017) funded by Kementerian Riset Teknologi dan Perguruan Tinggi through DRPM Universitas Indonesia.

References

[1] A. P. Ramirez, J. Phys. Condens. Matter **9**, 8171 (1997).
[2] J. Rhensius, C. A. F. Vaz, A. Bisig, S. Schweitzer, J. Heidler, H. S. Körner, A. Locatelli, M. A. Niño, M. Weigand, L. Méchin, F. Gaucher, E. Goering, L. J. Heyderman, and M. Kläui, Appl. Phys. Lett. **99**, 062508 (2011).
[3] M. Ziese, I. Vrejoiu, A. Setzer, A. Lotnyk, and D. Hesse, New J. Phys. **10**, 063024 (2008).
[4] K. J. O'Shea, K. Bova, D. McGrouther, and D. A. MacLaren, EPJ Web Conf. **75**, 05017 (2014).
[5] M. J. Donahue and D. G. Porter, OOMMF User's Guide Version 1.0, National Institute of Standard and Technology, Gaithersburg, MD (1999).
[6] T. L. Gilbert, IEEE Trans. Magn. **40**, 3443 (2004).
[7] M. Ziese, Phys. Status Solidi B **243**, 1383 (2006).
[8] N. Dao, M. J. Donahue, I. Dumitru, L. Spinu, S. L. Whittenburg, and J. C. Lodder, Nanotechnology **15**, S634 (2004).
[9] N. Vukadinovic, IEEE Trans. Magn. **38**, 2508 (2002).
[10] C. Kittel, Phys. Rev. **73**, 155 (1948).
[11] A. Aharoni, J. Appl. Phys. **83**, 3432 (1998).